Corner loading and curling stress analysis for concrete pavements — an alternative approach

Ying-Haur Lee, Ying-Ming Lee, and Shao-Tang Yen

Abstract: Since corner breaks are one of the major structural distresses in jointed concrete pavements, this research study mainly focuses on the determination of the critical bending stresses at the corner of the slab due to the individual and combination effects of wheel loading and thermal curling. A well-known slab-on-grade finite element program (ILLI-SLAB) was used for the analysis. The structural response characteristics of a slab corner were first investigated. Based on the principles of dimensional analysis, the dominating mechanistic variables were carefully identified and verified. A series of finite element factorial runs over a wide range of pavement designs was carefully selected and conducted. The resulting ILLI-SLAB corner stresses were compared with the theoretical Westergaard solutions, and adjustment factors were introduced to account for this discrepancy. Prediction equations for stress adjustments were developed using a modern regression technique (Projection Pursuit Regression). A simplified stress analysis procedure was proposed and implemented in a user-friendly computer program (ILLISTRS) to facilitate instant stress estimations and practical trial applications.

Key words: concrete (rigid) pavements, corner breaks, loading, thermal curling, corner stress.

Résumé : Puisque les ruptures d'angles sont l'une des principales causes de défaillance des chaussées faites de dalles de béton, ce projet de recherche se concentre principalement sur la détermination des contraintes critiques en flexion auxquelles est soumis l'angle de la dalle par effets combinés des sollicitations par les roues et de l'ondulation de nature thermique. Un programme par éléments finis bien connu de dalles sur sol (ILLI-SLAB) a été utilisé pour l'analyse. Les caractéristiques de la réponse structurelle de l'angle d'une dalle ont d'abord été étudiées. En se basant sur les principes de l'analyse dimensionnelle, les variables mécanistes dominantes ont été identifiées et vérifiées avec soin. Une série d'essais sur les facteurs des éléments finis, couvrant une large gamme de conception de chaussée, a été choisie et conduite avec soin. Les contraintes d'angle résultant du programme ILLI-SLAB ont été comparées aux solutions théoriques de Westergaard et des facteurs d'ajustement ont été introduits afin de rendre compte des divergences. Les équations de prédiction de l'ajustement des contraintes ont été développées au moyen d'une technique de régression moderne (Projection Poursuite Régression). Une procédure simplifiée d'analyse des contraintes a été proposée et mise en œuvre au sein d'un programme informatique convivial (ILLISTRS) dans le but de faciliter les estimations des contraintes instantanées et les expérimentations pratiques.

Mots clés : chaussée (rigide) en béton, ruptures d'angles, sollicitations, ondulation thermique, contrainte d'angle.

[Traduit par la Rédaction]

Introduction

Currently, most design procedures for concrete pavement thickness do not consider corner stress or curling stress in fatigue analysis, but many researchers have indicated that it should be considered to warrant a zero-maintenance thickness design (Lee and Lee 1996; Lee et al. 1997; Darter and Barenberg 1977). "Load repetition combined with loss of support and curling stresses" are usually recognized as the main causes for corner breaks (ASTM 1993; SHRP 1993). Given certain design, construction, and loading conditions corner breaks may occur due to fatigue damage at the slab corner over time.

The temperature differential through the slab thickness and the self-weight of the slab induce additional thermal curling stresses at the slab corner. For daytime curling condition, compressive curling stresses are induced at the top of the slab whereas tensile stresses occur at the bottom; or vice versa for nighttime curling condition. Curling stress may be quite large and cause the slab to crack or result in corner breaks when combined with only very few number of load repetitions. Darter and Barenberg (1977) surveyed the non-traffic loop of the AASHO road test and have found after 16 years most of the long slabs (12.19 m) had cracks, but not the 4.57-m slabs, probably because longer slabs have much greater curling stress than shorter slabs.

Two methods are often used to determine the stresses and deflections in concrete pavements: closed-form formulas and finite element computer programs. The formulas originally developed by Westergaard are for a single wheel load under the assumptions of infinite slab size and full contact at the

Received 6 December 2001. Revision accepted 8 April 2002. Published on the NRC Research Press Web site at http://cjce.nrc.ca on 1 August 2002.

Y.-H. Lee,[1] Y.-M. Lee, and S.-T. Yen. Department of Civil Engineering, Tamkang University, E725, 151 Ying-Chuan Road, Tamsui, Taipei, Taiwan 251.

Written discussion of this article is welcomed and will be received by the Editor until 31 December 2002.

[1]Corresponding author (e-mail: yinghaur@mail.tku.edu.tw).

 DOI: 10.1139/l02-033

slab–subgrade interface. To more accurately and realistically account for the effects of finite slab size and possible loss of subgrade support due to a temperature differential, finite element analyses should be used. Nevertheless, the difficulties of the required run time and complexity often prevent such analyses from being used in practical pavement designs.

The main objectives of this research work were to develop an alternative stress determination process, which can be incorporated into existing mechanistic-based design procedures with sufficient accuracy and efficiency for practical pavement designs. Specifically, this paper primarily focuses on the determination of critical bending stresses at the slab corner due to loading and curling to control the occurrence of corner breaks.

Closed-form solutions

Corner loading

In the analysis of a slab-on-grade pavement system, Westergaard has presented closed-form solutions for three primary structural response variables, i.e., slab bending stress, slab deflection, and subgrade stress, due to a single wheel load based on medium-thick plate theory. Based on the assumptions of an infinite or semi-infinite slab over a dense liquid foundation (Winkler foundation), Westergaard (1926) applied a method of successive approximations and obtained the following equations for a circular corner loading condition:

$$[1]\qquad \sigma_{wc} = \frac{3P}{h^2}\left[1-\left(\sqrt{2}\frac{a}{l}\right)^{0.6}\right]$$

$$\delta_{wc} = \frac{P}{kl^2}\left[1.1-0.88\left(\sqrt{2}\frac{a}{l}\right)\right]$$

where σ_{wc} is the critical corner stress, [FL^{-2}]; δ_{wc} is the critical corner deflection, [L]; P is the total applied wheel load, [F]; h is the thickness of the slab, [L]; a is the radius of the applied load, [L]; $l = (Eh^3/(12(1-\mu^2)k))^{0.25}$ is the radius of relative stiffness of the slab–subgrade system, [L]; k is the modulus of subgrade reaction, [FL^{-3}]; E is the modulus of elasticity of the concrete slab, [FL^{-2}]; and μ is the Poisson's ratio of the concrete. The [F] represents the primary dimension for force and [L] represents the primary dimension for length. The distance to the point of maximum stress along the corner angle bisector was found to be roughly

$$[2]\qquad X_1 = 2\sqrt{\sqrt{2}al} \cong 2.38\sqrt{al}$$

The above stress and deflection equations were derived using a simple approximate process and have been debated and led to numerous revisions such as those proposed by Bradbury, Kelly, Teller and Sutherland, Spangler, and Pickett over the years (Ioannides 1984). Despite this argument, Ioannides et al. (1985) later has indicated that the ILLI-SLAB finite element results closely fall between those predicted by Westergaard and Bradbury. The ILLI-SLAB stresses are the minor principal (tensile) stresses occurring at the top fiber of the slab corner. Thus, Westergaard's approximation was still relatively good.

Thermal curling

Considering curling stresses caused by a linear temperature differential on a concrete slab over a dense liquid foundation, Westergaard (1927) developed equations for three slab conditions (i.e., infinite, semi-infinite, and an infinite long strip). The interior curling stress, σ_{c0} ([FL^{-2}]), for an infinite slab is

$$[3]\qquad \sigma_{c0} = \frac{E\alpha\Delta T}{2(1-\mu)}$$

where α is the thermal expansion coefficient ([T^{-1}]) and ΔT is the temperature differential through the slab thickness ([T]). The [T] represents the primary dimension for temperature.

Bradbury (1938) later expanded Westergaard's bending stress solutions for a slab with finite dimensions in both transverse and longitudinal directions. The edge and interior curling stresses, σ_{ce} and σ_{ci} ([FL^{-2}]), can be determined by

$$\sigma_{ce} = \frac{CE\alpha\Delta T}{2}$$

$$[4]\qquad = \frac{E\alpha\Delta T}{2}\left[1-\frac{2\cos\lambda\cosh\lambda}{\sin 2\lambda+\sinh 2\lambda}(\tan\lambda+\tanh\lambda)\right]$$

$$\sigma_{ci} = \frac{E\alpha\Delta T}{2}\left[\frac{C_1+\mu C_2}{1-\mu^2}\right]$$

where $\lambda = B/(l\sqrt{8})$, B is the finite slab width or length ([L]), and C_1 and C_2 are the curling stress coefficients for the desired and perpendicular directions. However, there exists no explicit closed-form solution for corner stress.

Loading plus thermal curling

Considering the combined effect of loading plus curling, Bradbury further analyzed the curling stress on a diagonal corner section located at or near the section at which the maximum loading stress occurs, i.e., the location determined by eq. [2]. Consequently, Bradbury derived the following approximate corner curling stress:

$$[5]\qquad \sigma_{ct} = \frac{E\alpha\Delta T}{3(1-\mu)}\sqrt{\frac{a}{l}}$$

where σ_{ct} is the maximum curling stress to be combined with the maximum stress induced by loading at the corner, [FL^{-2}]. Even though both Westergaard and Bradbury suggested that this effect could be treated as "a simple matter of addition" in most cases, many investigators indicated that such an action may not always be conservative because of the possible loss of subgrade support and the violation of full contact assumption (Ioannides et al. 1985; Korovesis 1990).

Finite element computer program

The analysis of finite slab length and width effect was not possible until the introduction of finite element models. The basic tool for this analysis is the ILLI-SLAB finite element computer program, which was originally developed in 1977 and has been continuously revised and expanded at the University of Illinois over the years. The ILLI-SLAB model is

based on the classical medium-thick plate theory, which uses the 4-noded 12-degree-of-freedom plate bending elements. The Winkler foundation assumed by Westergaard is modeled as a uniform, distributed subgrade through an equivalent mass foundation. Curling analysis was not implemented until versions after June 1987. Heinrichs et al. (1989) and Huang (1993) indicated that the ILLI-SLAB model had extensive checking, revisions, and verifications by many researchers, could structurally model many key design factors of importance, and was more free of errors than any other available computer program for rigid pavements. Huang also reached similar conclusions through many extensive comparison studies among the KENSLABS, ILLI-SLAB, and JSLAB models. With some modifications to the original codes, the ILLI-SLAB model (Korovesis 1990) was successfully recompiled using Microsoft FORTRAN PowerStation (Microsoft Taiwan Corp. 1994). The applicability of the ILLI-SLAB finite element program for stress estimation was conducted and verified through comparisons of the resulting ILLI-SLAB stresses and the actual field measurements from some test sections of Taiwan's second northern highway, the AASHO road test, and the Arlington road test.

Characteristics of corner stresses

The structural response characteristics of a slab subjected to the individual and combination effects of a single-wheel corner load and a linear temperature differential were first investigated. A preliminary analysis under this study has also indicated that the location of the maximum combined stress due to loading plus curling varies from case to case. Thus, unlike the analysis of interior or edge stresses where the maximum stresses occur at the same critical center or mid-slab location, the analysis of corner stresses is probably the most difficult one among these three cases. As illustrated in Fig. 1*a*, the following parameters were also assumed: $L/l = 7$, $W/l = 7$, $l = 106.3$ cm, $h = 30.5$ cm, $k = 65.0$ kPa/mm, $E = 34.5$ GPa, $\gamma = 2410$ kg/m^3, and $\mu = 0.15$. Note that $a/l = 0.1$ and $c = 18.8$ cm were selected for the given corner load and $\Delta T = -11.1$°C and $\alpha = 9.9 \times 10^{-6}$/°C were chosen for the temperature differential.

Loading only

Under this case study, a tire pressure, p, of 537 kPa was selected and the loaded area was equal to 19 × 19 cm^2. The resulting maximum tensile stress was 439 kPa, located at (x, y) = (56.6 cm, 56.6 cm). This point is equivalent to a distance of 79.0 cm along the corner angle bisector. According to Westergaard's equation (eq. [1]), the corresponding maximum corner stress was 435 kPa at a distance of X_1 = 80.5 cm. Thus, the ILLI-SLAB results agree very well with Westergaard's solutions for this case.

Upward curling only

In this case, $\Delta T = -11.1$°C and $\alpha = 9.9 \times 10^{-6}$/°C were assumed. A more realistic assumption of partial contact at the slab–subgrade interface was allowed and the self-weight of the concrete slab was also considered. For the nighttime condition when the temperature on the top of the slab was lower than at the bottom of the slab (or $\Delta T < 0$), an upward curling occurred. Due to the self-weight of the slab, tensile stresses occurred on the top and compressive stresses at th bottom of the slab. It is worth mentioning, however, that th maximum tensile stress (1859 kPa) occurred at the center o the slab rather than the corner.

Large loading plus small curling

To illustrate the combination effect, a relatively large an hypothetical tire pressure, p, of 5374 kPa together with th same temperature differential was assumed in this case Since nighttime (negative ΔT) curling condition will result i additional tensile stress at the top fiber of the slab, this stud is only limited to the most critical case of corner loadin plus nighttime curling. The resulting maximum tensile stres was 4711 kPa, located at (x, y) = (10 cm, 102 cm), which i equivalent to a distance of 102 cm along the corner angle bi sector. This result is approximately equal to the sum of 1(times of the stress due to the loading-only case (p = 537 kPa) and the tensile stress at the specified point due t curling alone.

Small loading plus large curling

This case assumes a tire pressure, p, of 537 kPa togethe with the same negative linear temperature differential. Th resulting maximum tensile stress was 2001 kPa, located a (353 cm, 353 cm) which is equivalent to a distance, X_1, o 499.4 cm along the diagonal line. In fact, it was very clos to the center of the slab and the magnitude of the stress wa approximately equal to the sum of both individual effects a that point.

Medium loading plus medium curling

This case assumes a tire pressure, p, of 1399 kPa such tha the resulting loading-only stress will have about the sam magnitude as the aforementioned curling-only effect. The resulting maximum combined tensile stress was 2110 kPa, located at (304.8 cm, 304.8 cm). This critical stress location was far away from the point of X_1 = 80.5 cm as determined by Westergaard's equation. The resulting maximum tensile stress was less than the summation of both individual effects using the principle of superposition.

Location of the maximum combined stresses

The individual and combined stress contour plots of all cases are shown in Figs. 1*b*–1*f*, respectively. In summary, if the temperature differential is relatively small combined with a large corner load, the critical stress location is very close to Westergaard's maximum load stress location. However, if the temperature differential is very large along with a very small corner load, the critical stress location may shift toward and up to the center of the slab. For the combined effects of medium loading and medium curling, the maximum stress location falls between them. Thus, the location of the maximum combined stresses due to loading plus curling will fall within the Westergaard's location and the center of the slab along the corner angle bisector as shown in Fig. 2. Furthermore, the corner stress along the line of a 1/4 circle centered at the very corner of the slab also shows about the same magnitude at most locations. This may also help to explain the mechanism of the development of corner breaks.

Research continues with special attentions to this different critical stress location problem. Consequently, necessary

Fig. 1. Distribution of the tensile stresses (kPa) on the top of the slab: (*a*) case study of corner stress analysis, (*b*) loading only, (*c*) curling only (nighttime condition), (*d*) large loading plus small curling, (*e*) small loading plus large curling, and (*f*) medium loading plus medium curling.

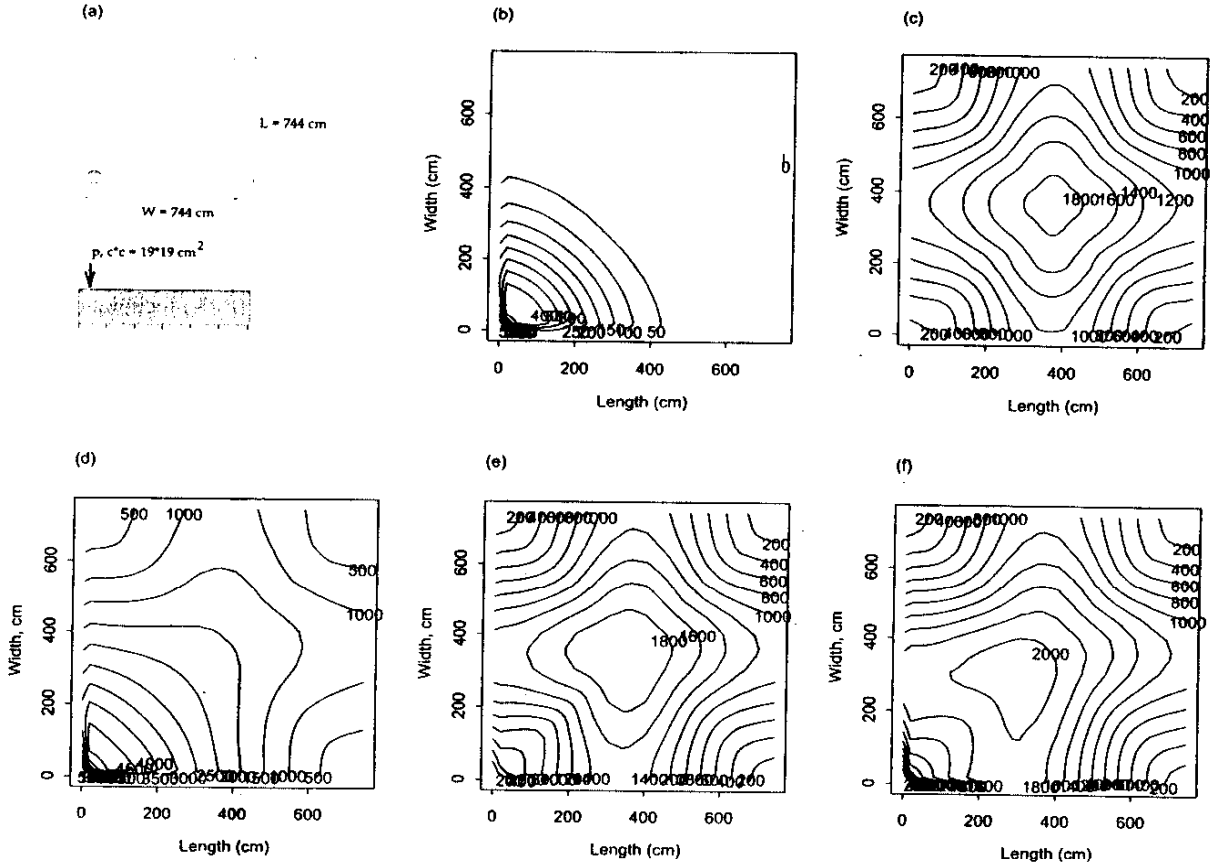

modifications were made to the existing ILLI-SLAB codes to facilitate the search of critical stresses and locations along the corner angle bisector or the diagonal nodes up to the center of the slab for the remaining analyses.

Identification of dimensionless mechanistic variables

When there exist no closed-form solutions for the selected theoretical analysis tools or when analyzing most empirical but practical engineering problems, the principles of dimensional analysis is often used. The principles of dimensional analysis treat a theoretical equation in non-dimensional form, which is composed of a set of many dimensionless parameters representing a concise interrelationship among any complicated combinations of all input variables with dimensions. Thus, the number of parameters and data analysis time and costs may be reduced dramatically.

Westergaard's closed-form solutions were based on the ideal assumptions of an infinite or semi-infinite slab size, full contact at the slab–subgrade interface, and a single loaded area. Through the use of the principles of dimensional analysis, earlier investigators (Ioannides et al. 1985) have demonstrated that theoretical Westergaard solutions and finite element solutions for three primary structural responses due to a single wheel load can be concisely defined by the following expression for a constant Poisson's ratio (usually $\mu \approx 0.15$):

Fig. 2. Expected maximum stress location.

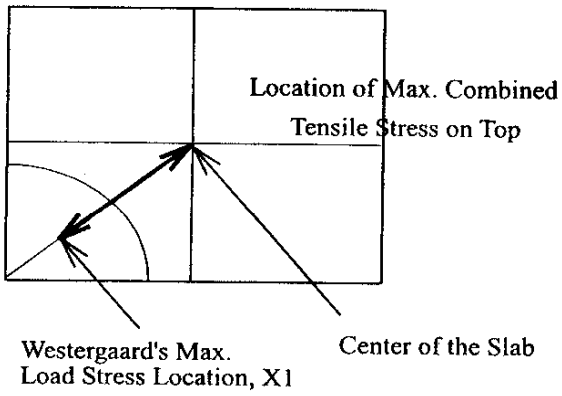

$$[6] \quad \frac{\sigma h^2}{P}, \frac{\delta k l^2}{P}, \frac{q l^2}{P} = f_1\left(\frac{a}{l}, \frac{L}{l}, \frac{W}{l}\right)$$

where σ and q are the slab bending stress and the vertical subgrade stress, respectively, [FL^{-2}]; δ is the slab deflection, [L]; f_1 is a function of a/l, L/l, and W/l; and L and W are finite slab length and width, [L]. Note that the variables in both sides of the expression are all dimensionless. The dependent variables are $\sigma h^2/P$, $\delta kl^2/P$, and ql^2/P, which are only dominated by the normalized load radius (a/l) and the normalized slab length and width (L/l and W/l) rather than the other input parameters, such as E, h, k, and a.

Furthermore, according to recent research by Lee and Darter (1994*a*) for the stress analysis at the very edge of the slab, concise relationships have been proposed and numerically verified through a series of finite element runs. The dimensionless mechanistic variables due to the effects of thermal curling alone and loading plus curling for a constant Poisson's ratio are

$$\frac{\sigma}{E}, \frac{\delta h}{l^2}, \frac{qh}{kl^2} = f_2\left(\alpha\Delta T, \frac{L}{l}, \frac{W}{l}, \frac{\gamma h^2}{kl^2}\right)$$

$$[7] \quad \frac{\sigma}{E}, \frac{\delta h}{l^2}, \frac{qh}{kl^2} = f_3\left(\frac{a}{l}, \alpha\Delta T, \frac{L}{l}, \frac{W}{l}, \frac{\gamma h^2}{kl^2}, \frac{ph}{kl^4}\right)$$

$$D_\gamma = \frac{\gamma h^2}{kl^2}, \qquad D_p = \frac{ph}{kl^4}$$

where γ is the unit weight of the concrete slab, [FL^{-3}]; and f_2 and f_3 are functions for curling alone and curling plus loading, respectively. Also note that D_γ is defined as the relative deflection stiffness due to the self-weight of the concrete slab and the possible loss of subgrade support, whereas D_p is the relative deflection stiffness due to the external wheel load and the loss of subgrade support.

Conceptually, the above relationship should be applicable to any given loading conditions. To numerically verify the above relationships for the individual and combined corner stresses due to loading and thermal curling in this study, several series of factorial finite element runs were performed. While keeping the dominating mechanistic variables constant but changing any other individual input variables to different values, the finite element results have indicated that the aforementioned relationship also hold for the corner condition (Lee et al. 1996).

Development of corner loading and curling stress prediction models

A series of finite element factorial runs were performed based on the dominating mechanistic variables identified. Several BASIC programs were written to automatically generate the finite element input files and summarize the desired outputs. The finite element mesh was generated according to the guidelines established in earlier studies (Ioannides 1984). The projection pursuit regression technique introduced by Friedman and Stuetzle (1981) was used for the development of the following three stress prediction models:

1. Case I (loading only): Full contact assumption was applied, no temperature differential existed, and the self-weight of the slab was neglected.
2. Case II (loading plus self-weight): Partial contact at the slab–subgrade interface was allowed. Although the temperature differential was set to zero ($\Delta T = 0$), the self-weight of the slab was considered in this case.
3. Case III (loading plus nighttime curling): A more general case for loading plus curling. Partial contact was allowed, and both the temperature differential ($\Delta T < 0$) and the self-weight of the slab were considered.

The stress prediction models were represented in the form of adjustment factors (R), which were specially chosen to satisfy theoretical boundary conditions. As a result, R values range from 0 to 1, or at most up to an approximate maximum value of 1.2 for all three cases, which may also help to control the prediction accuracy.

Application of the new predictive modeling technique

Projection pursuit regression (PPR) techniques introduced by Friedman and Stuetzle (1981) strive to model the response surface (y) as a sum of nonparametric functions of projections of the predictor variables (x) through the use of local smoothing techniques. Assuming there is a true model:

$$[8] \quad y = \bar{y} + \sum_{m=1}^{M_0} \beta_m \phi_m(a_m^T x) + \varepsilon$$

where $x = (x_1, x_2, \cdots, x_p)^T$ denotes the vector of predictor variables, $\bar{y}$ is the expected (or mean) value of response variable, β_m is the regression coefficient, and ε is the residual or random error. The PPR algorithm strives to minimize the mean squared residuals over all possible combinations of β_m, ϕ_m, and a_m values. Conceptually, the explanatory variables x are projected onto the direction vectors $a_1, a_2, \cdots, a_m$, to get the lengths of the projections $a_m^T x$, where $m = 1, \cdots, M_0$. An optimization technique is also used to find the best combinations of nonlinear transformations $\phi_1, \phi_2, \cdots, \phi_m$ for the multi-dimensional response surface. The $\phi_m(a_m^T x)$ represents the unknown nonparametric transformation functions of the estimated projected lengths $a_m^T x$.

As proposed by Lee and Darter (1994*b*), the two-step modeling approach using the PPR technique was utilized for the development of prediction models. Through the use of local smoothing techniques, the PPR attempts to model a multi-dimensional response surface as a sum of several nonparametric functions of projections of the explanatory variables. The projected terms are essentially two-dimensional curves, which can be graphically represented, easily visualized, and properly formulated. Piecewise linear or nonlinear regression techniques were then used to obtain the parameter estimates for the specified functional forms of the predictive models. This algorithm is available in the S-PLUS statistical package (Statistical Sciences Inc. 1995). A practical predictive modeling example using this approach can be found in the literature (Lee and Darter 1994*b*).

Case I: loading only

In Case I, a single wheel load was applied at the slab corner. There was no thermal curling effect and the Westergaard's full subgrade support was assumed in this case. Based on previous investigation (Ioannides et al. 1985), Westergaard's infinite slab assumption may be achieved if the normalized slab length (L/l) is equal to 5.0 or more. Thus, a more conservative value of 7.0 for both L/l and W/l was selected to ensure infinite slab condition. The

Table 1. Proposed prediction models for corner stress adjustments.

Finite slab size	$R_{2a} = 1.030 + 0.030\Phi_1 + 0.045\Phi_2$
	$\Phi_1 = 92.145 - 149.276(A1) + 59.747(A1)^2$
	$\Phi_2 = \begin{cases} -6.034 + 23.128(A2) - 22.022(A2)^2 & \text{if } A2 \le 0.6 \\ -0.117 + 0.375(A2) & \text{if } 0.6 < A2 \end{cases}$
	$A1 = 0.8272x1 - 0.1219x2 + 0.0002x3 + 0.5485x4$
	$A2 = -0.9034x1 + 0.2973x2 - 0.0118x3 - 0.3088x4$
	$X1 = [x1, x2, x3, x4] = \left[\frac{a}{l}, \frac{L}{l} + \frac{W}{l}, \frac{L}{l}\left(\frac{W}{l}\right), \sqrt{\frac{L}{l}} + \sqrt{\frac{W}{l}}\right]$
Loading plus self-weight ($\Delta T = 0$)	$R_{2b} = 0.9949 + 0.17037\Phi_1 + 0.03020\Phi_2$
	$\Phi_1 = \begin{cases} -0.85525 + 15.53557(A1) + 1.71139(A1)^2 & \text{if } A1 \le 0.1 \\ 0.24816 + 0.28387(A1) - 0.06692(A1)^2 & \text{if } A1 > 0.1 \end{cases}$
	$\Phi_2 = \begin{cases} -0.93998 + 3.72027(A2) + 11.13839(A2)^2 & \text{if } A2 \le 0.18 \\ -2.93892 + 16.93742(A2) & \text{if } A2 > 0.18 \end{cases}$
	$A1 = -0.95810x1 + 0.03604x2 + 0.28368x3 - 0.00231x4 - 0.00033x5 - 0.00236x6 - 0.00144x7 + 0.01621x8$
	$A2 = 0.99699x1 - 0.02358x2 + 0.05534x3 - 0.00265x4 + 0.00055x5 + 0.01611x6 - 0.00041x7 - 0.04602x8$
	$X = [x1, x2, \ldots, x8] = \left[\frac{a}{l}, \frac{L}{l}, \frac{a}{l}\left(\frac{L}{l}\right), \left(\frac{a}{l}\right)\text{DP}, \text{DP}, \text{DG}, \frac{\text{DP}}{\text{DG}}, \left(\frac{a}{l}\right)\text{DG}\right]$
	Limits: $0.05 \le a/l \le 0.3$, $2 \le L/l \le 15$, $W/l = L/l$, $1 \le \text{DG} \le 10$, $2 \le \text{DP} \le 130$, $\text{DG} = D_\gamma \times 10^5$, $\text{DP} = D_p \times 10^5$
Loading plus nighttime curling ($\Delta T < 0$)	$R_T = 0.2548 + 0.3076\Phi_1 + 0.1058\Phi_2 + 0.05934\Phi_3$
	$\Phi_1 = \begin{cases} -0.28987 + 0.02840(A1) & \text{if } A1 \le 0 \\ -0.22478 + 0.40575(A1) & \text{if } A1 > 0 \end{cases}$
	$\Phi_2 = \begin{cases} -1.46318 + 0.39571(A2) + 0.00231(A2)^2 - 0.00155(A2)^3 & \text{if } A2 \le 15 \\ 5.06880 - 0.32371(A2) & \text{if } A2 > 15 \end{cases}$
	$\Phi_3 = \begin{cases} 0.73250 + 0.74738(A3) & \text{if } A3 \le 0 \\ 0.68128 + 0.25940(A3) & \text{if } A3 > 0 \end{cases}$
	$A1 = -0.04291x1 + 0.56894x2 - 0.43915x3 + 0.05771x4 - 0.12609x5 + 0.02591x6 + 0.01885x7 - 0.15518x8 + 0.50270x9 - 0.01229x10 + 0.31315x11 - 0.00903x12 + 0.00649x13 + 0.28839x14 - 0.04413x15 + 0.03329x16 - 0.00002x17$
	$A2 = -0.02058x1 + 0.83621x2 - 0.36689x3 + 0.25029x4 - 0.16713x5 + 0.04484x6 + 0.07580x7 + 0.03647x8 - 0.09497x9 + 0.00207x10 - 0.04534x11 - 0.00721x12 + 0.0007x13 + 0.23382x14 + 0.01217x15 + 0.01038x16 - 0.00016x17$
	$A3 = 0.04637x1 - 0.44327x2 + 0.39157x3 + 0.47010x4 - 0.12200x5 - 0.00537x6 - 0.00851x7 - 0.01246x8 - 0.48078x9 + 0.00443x10 + 0.01520x11 + 0.00322x12 - 0.00293x13 + 0.42430x14 + 0.01628x15 - 0.01370x16 + 0.00007x17$
	$X = [x1, x2, \ldots, X17] = [a/l, L/l, \text{ADT}, (a/l)(L/l), (a/l)\text{ADT}, (L/l)\text{ADT}, (a/l)(L/l)\text{ADT}, \text{DP}, \text{DG}, \text{DP(DG)}, \text{DP}(a/l), \text{DP}(L/l), \text{DP(ADT)}, \text{DG}(a/l), \text{DG}(L/l), \text{DG(ADT)}, \text{ADT}(L/l)(a/l)(\text{DP})(\text{DG})]$

following factorial finite element runs were conducted: a/l = 0.05, 0.1, 0.2, 0.3; L/l = 2, 3, 4, 5, 6, 7; W/l = 2, 3, 4, 5, 6, 7; and $L/l \ge W/l$.

Since L/l and W/l are analogous, a total of 84 runs only were necessary if slab length was chosen to be greater than slab width. The resulting maximum corner stresses were obtained and compared to the Westergaard solution. Prediction model was developed for the adjustment factor (R) and summarized in Table 1. This prediction model is also applicable to a larger slab when the upper bound value of 7.0 is used for the normalized slab length or width (L/l, W/l).

Case II: loading plus self-weight

In Case II, the combination effect of a single wheel load and the self-weight of the slab at the slab corner was considered. A linear temperature differential ΔT was assumed zero in such a case. Therefore, the ILLI-SLAB program was modeled to allow partial contact at the slab–subgrade interface, since a complete full factorial of all the six dimensionless parameters, which requires a tremendous amount of computer time, is not feasible. Thus, the following factorial finite element runs were conducted: a/l = 0.05, 0.1, 0.2, 0.3; L/l = 2, 3, 4, 5, 7, 9, 11, 13, 15; $W/l = L/l$; and $\alpha\Delta T = 0$.

Notice that a squared slab up to a maximum normalized slab length (L/l) of 15, which may satisfy Westergaard's infinite slab assumption for thermal curling analysis. Furthermore, to account for D_γ and D_p effects without increasing the number of finite element runs, the above factorial runs were randomized by these two factors for different a/l values using the concept of experimental design. For a/l = 0.05, 0.10, 0.20, and 0.30, the following combinations of (DG, DP) = (D_γ, D_p) × 10^5 factorial runs were conducted: (1, 2), (10, 30), (7, 130); (4, 30), (7, 70), (4, 130); (4, 2), (7, 30), (10, 70); and (1, 2), (10, 70), (1, 130), respectively.

After conducting considerable amounts of PPR trials, predictive model was developed for stress adjustment factor (R) and summarized in Table 1.

Case III: loading plus nighttime curling

Cases II and III all consider the combination effect of a single wheel load and the self-weight of the slab at the slab corner. However, a nighttime linear temperature differential ($\Delta T < 0$) was assumed different from zero in this case. Therefore, other than ΔT was selected differently, the aforementioned factorial design of finite element runs for Case II was also adopted for this case. The ΔT values were selected as follows: ΔT = −5.5, −11.1, −16.7, −22.2°C ($\alpha = 9.9 \times 10^{-6}$/°C). Thus, a total of 432 factorial finite element runs were conducted for this analysis. The following adjustment factor (R) was carefully selected to account for the theoretical difference between Case II and Westergaard's interior curling stress solutions:

$$[9a] \quad R = \frac{\sigma_{i(CaseIII)} - \sigma_{i(CaseII)}}{\sigma_{c0}}$$

or

$$[9b] \quad \sigma_{i(CaseIII)} = \sigma_{i(CaseII)} + R\sigma_{c0}$$

where σ_i is the combined maximum finite element corner stress ([FL^{-2}]) and σ_{c0} is defined by eq. [3]. By using the PPR algorithm, the predictive model for R was developed and summarized in Table 1.

Verification of the proposed corner stress prediction models

To further verify the applicability of the proposed prediction models for all three cases, totally different sets of database were created. The following input parameters were chosen: E = 20.7, 37.9, 55.1 GPa; k = 13.5, 67.8, 135.5 kPa/mm; L = 3.05, 6.10, 9.15 m; h = 20.3, 30.5, 40.6 cm; ΔT = 0, −11.1, −16.7, −22.2°C ($\alpha = 9.9 \times 10^{-6}$/°C). Note that the other pertinent input parameters are c = 25.4 cm, a = 14.33 cm, P = 40 kN, p = 620 kPa, μ = 0.15, γ = 2410 kg/m^3, and $W = L$. This will result in a total of 81 ILLI-SLAB runs with the ranges of a/l = 0.07 ~ 0.21, L/l and W/l = 1.4 ~ 15.9 for Case I and Case II, and a total of 243 ILLI-SLAB runs for Case III.

For values outside the specified limits of the prediction model, the upper or lower bounds were applied for the analysis. The predicted stresses were plotted against the resulting ILLI-SLAB corner stresses (Lee et al. 1996; Lee and Lee 1995). Almost perfect agreement of the stress predictions for Case I and Case II was noted. There exists, however, some minor discrepancy for Case III due to the critical location of minor principal stress changes from case to case. The possibility of incorporating the location of critical stress occurrence into the process of stress estimation should be further investigated for future improvement.

Effect of a second subbase layer

The subgrade k value was originally developed for characterizing the support of natural soils with fairly low shear strength. Substantially higher k values were obtained based on plate tests on the top of granular and stabilized base layers. The FAA airfield pavement design approach as well as the current PCA design procedure and the 1986 AASHTO Guide for concrete highway pavements all adopt the concept of a composite "top-of-the-base" k-value for design, though many researchers have indicated the inadequacy of this concept. Through the review of results from several field studies and the examination of the k-value methods introduced in the 1986 AASHTO Guide, "it is recommended that k values be selected for natural soil materials, and that base layers be considered in concrete pavement design in terms of their effect on the slab response, rather than their supposed effect on k value" (Hall et al. 1995; Darter et al. 1995). Improved guidelines for k-value selection from a variety of methods are provided in the 1998 Supplement Guide for the design of concrete pavement structures accordingly.

Even though the concept of transformed section was frequently utilized to account for the stress reduction factor (R_5) due to a bonded or unbonded second layer, it was sometimes found misused in the literature (Salsilli-Murua 1991; Lee et al. 1997; Kuo 1994). Subsequently, a more complete treatment of this concept is presented as follows.

Stress adjustment due to a second unbonded subbase layer

Following the formulation given by Tabatabai-Raissi (1977), a system of two unbonded layers is transformed into an equivalent single layer based on the assumption of same total bending moment as shown in Fig. 3. The maximum bending moment per unit width of a given single layer is equal to $\sigma h^2/6$. Assuming both layers have the same Poisson's ratio, the relationship of the top layer stress (σ_1) and the bottom layer stress (σ_2), the total bending moment per unit width (M_T), and the effective thickness (h_{eff}) can be expressed by

$$[10] \quad \frac{\sigma_1}{\sigma_2} = \frac{E_1 h_1}{E_2 h_2}$$

$$[11] \quad M_T = \frac{\sigma_1}{6}\left[h_1^2 + \left(\frac{E_2 h_2}{E_1 h_1}\right)h_2^2\right] = \frac{\sigma_1 h_{eff}^2}{6}$$

$$[12] \quad h_{eff} = \sqrt{h_1^2 + \left(\frac{E_2 h_2}{E_1 h_1}\right)h_2^2}$$

in which E_1 and E_2 are the modulus of elasticity of the slab and subbase layers, respectively, and h_1 and h_2 are the thickness of the slab and subbase layers, respectively.

Fig. 3. Transforming two unbonded layers into an equivalent single layer: (*a*) single layer, (*b*) two unbonded layers, and (*c*) equivalent single layer.

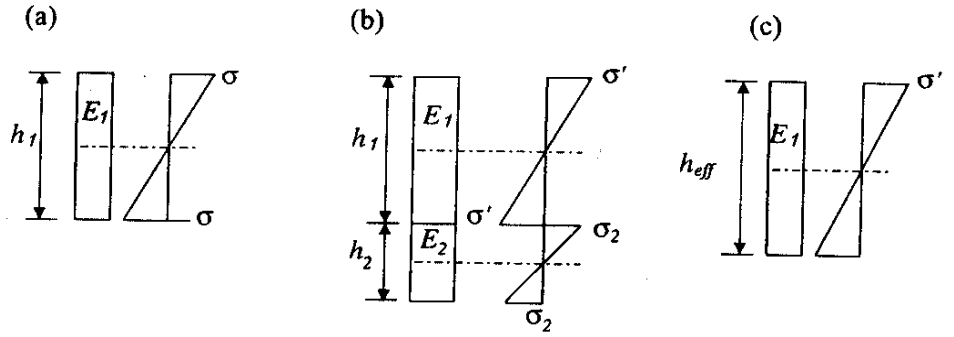

Fig. 4. Considering two bonded layers as an equivalent single layer: (*a*) two bonded layers, (*b*) strain, and (*c*) stress.

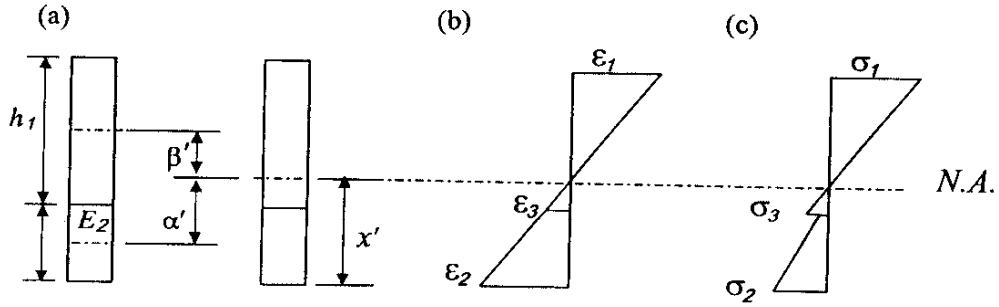

Alternatively, using the equivalent moment of inertia per unit width (I_{eff}) for the transformed section with modulus E_1, the effective thickness (h_{eff}) and the slab bending stress (σ_{unbond}) of the two-layer unbonded system can be determined by

$$[13] \quad I_{eff} = I_1 + \left(\frac{E_2}{E_1}\right) I_2 = \frac{h_1^3}{12} + \left(\frac{E_2}{E_1}\right)\frac{h_2^3}{12} = \frac{h_{eff}^3}{12}$$

$$[14] \quad h_{eff} = \sqrt[3]{h_1^3 + \left(\frac{E_2}{E_1}\right)h_2^3}$$

$$[15] \quad \sigma_{unbond} = \sigma_{wc}\left(\frac{h_1}{h_{eff}}\right)\left(\frac{\sigma'}{\sigma}\right) = \sigma_{wc}R_5$$

in which σ and σ' are the slab bending stress of a single layer and the equivalent single layer to be determined by eq. [1], respectively. Also note that the multiplication factor of h_1/h_{eff} is necessary to adjust the stress proportionally according to Figs. 3*b* and 3*c*.

Stress adjustment due to a second bonded subbase layer

As for the case of two bonded layers, considering a cross section of the slab–subbase system as an equivalent single layer, its corresponding strain and stress relationships are shown in Fig. 4. The location of the neutral axis is defined at a distance x from the bottom of the second layer:

$$[16] \quad x' = \frac{E_1h_1^2 + 2E_1h_1h_2 + E_2h_2^2}{2(E_1h_1 + E_2h_2)}$$

in which α and β are the distances of the neutral axis from the middle surfaces of the second layer and the top layer, respectively ($\alpha' = x' - h_2/2$, $\beta' = h_2 + h_1/2 - x'$).

By converting this system into an equivalent unbonded system as shown in Fig. 5, the equivalent top layer thickness (h_{1f}) and bottom layer thickness (h_{2f}) become $h_{1f} = \sqrt[3]{h_1^3 + 12h_1\beta'^2}$ and $h_{2f} = \sqrt[3]{h_2^3 + 12h_2\alpha'^2}$. Similarly, using the equivalent moment of inertia per unit width (I_{eff}) for the transformed section with modulus E_1, the effective thickness (h_{eff}) and the slab bending stress (σ_{bond}) of the two-layer bonded system can be determined by the following expression:

$$[17] \quad h_{eff} = \sqrt[3]{h_{1f}^3 + \left(\frac{E_2}{E_1}\right)h_{2f}^3}$$

$$[18] \quad \sigma_{bond} = \sigma_{wc}\left[\frac{2(x' - h_2)}{h_{eff}}\right]\left(\frac{\sigma'}{\sigma}\right) = \sigma_{wc}R_5$$

in which σ and σ' are the slab bending stress of a single layer and the equivalent single layer to be determined by eq. [1], respectively. Also note that the multiplication factor of $2(x' - h_2)/h_{eff}$ is necessary to adjust the stress proportionally according to Figs. 5*a* and 5*b*.

The applicability of the stress adjustment equations [15] and [18] was further verified through comparison of the results of a series of ILLI-SLAB finite element runs with excellent agreements.

Fig. 5. Transforming two bonded layers into two unbonded layers: (*a*) converting into two unbonded layers and (*b*) stress.

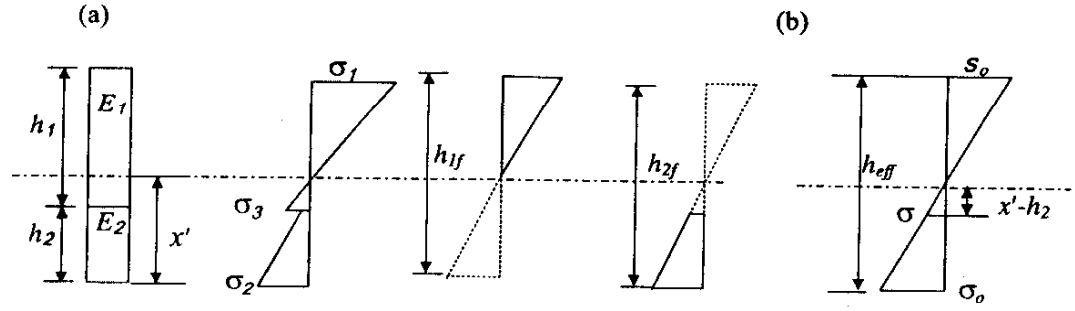

Simplified corner stress analysis procedures

In reality, jointed concrete pavements consist of many single finite concrete slabs jointed by aggregate interlock, dowel bars, or tie bars, and traffic loading may be in the forms of dual wheel, tandem axle, or tridem axle. A widened outer lane may also shift the wheel loading away from Westergaard's critical loading locations. A tied concrete shoulder or a second bonded or unbonded layer may also result in different degrees of stress reductions. To account for these effects under the loading-only condition, the following relationship has been identified through many intensive finite element studies for a constant Poisson's ratio (usually $\mu \approx 0.15$) (Lee and Lee 1996; Lee 1993; Lee et al. 1996):

$$[19] \quad \frac{\sigma h^2}{P}, \frac{\delta k l^2}{P}, \frac{q l^2}{P}, = f\left[\frac{a}{l}, \frac{L}{l}, \frac{W}{l}, \frac{s}{l}, \frac{t}{l}, \frac{D_0}{l}, \frac{\mathrm{AGG}}{kl}, \left(\frac{h_{\mathrm{eff}}}{h_1}\right)^2\right]$$

where σ and q are slab bending stress and vertical subgrade stress, respectively, [FL^{-2}]; δ is the slab deflection, [L]; P is the wheel load, [F]; h is the thickness of the slab, [L]; a is the radius of the applied load, [L]; l is the radius of relative stiffness of the slab–subgrade system, [L]; k is the modulus of subgrade reaction, [FL^{-3}]; L and W are the length and width of the finite slab, respectively, [L]; s is the transverse wheel spacing, [L]; t is the longitudinal axle spacing, [L]; D_0 is the offset distance between the outer face of the wheel and the slab edge, [L]; AGG is the aggregate interlock factor, [FL^{-2}]; h_{eff} is the effective thickness of two unbonded layers, [L]; h_1 and h_2 are the thickness of the top slab and of the bottom slab, respectively, [L]; and E_1 and E_2 are the concrete modulus of the top slab and of the bottom slab, respectively, [FL^{-2}]. Note that the variables in both sides of the expression are all dimensionless.

Since no thermal curling effect was considered in the above relationship, the assumption of full contact at the slab–subgrade interface and the principle of superposition may be applied to the analyses. Thus, the above relationship can be broken down to a series of simple analyses for each individual effect. The adjustment factors have been separately developed by Lee and Lee (1996) for stress reduction due to each different corner loading condition and are summarized in Table 2 for completeness of the discussion.

Consequently, the following equation was proposed to account for the combined effects of different material properties, finite slab sizes, gear configurations, and environmental effects (e.g., temperature differentials) for corner stress estimations (Lee and Lee 1996; Lee et al. 1996):

$$[20] \quad \sigma_c = \sigma_{wc} R_1 R_2 R_3 R_4 R_5 + R_T \sigma_{c0}$$

where σ_c is the corner stress prediction, [FL^{-2}]; σ_{wc} is Westergaard's closed-form corner stress solution as given in eq. [1], [FL^{-2}]; σ_{c0} is Westergaard's interior curling stress for an infinite slab shown in eq. [3], [FL^{-2}]; R_1 is the adjustment factor for different gear configurations, including dual-wheel, tandem axle, and tridem axle; $R_2 = R_{2a}$ or R_{2b}; R_{2a} is the adjustment factor for finite slab length and width for the loading-only condition, i.e., Case I; R_{2b} is the adjustment factor for finite slab length and width for the condition of loading plus curling but $\Delta T = 0$ to allow partial contact at the slab–subgrade interface, i.e., Case II; R_3 is the adjustment factor for a tied concrete shoulder; R_4 is the adjustment factor for a widened outer lane; R_5 is the adjustment factor for a bonded/unbonded second layer using eqs. [15] and [18]; and R_T is the adjustment factor for the combined effect of loading plus nighttime curling, i.e., Case III; also note that the adjustment factors R_T and R_{2b} should be used together for higher accuracy.

Development of the ILLISTRS program

To facilitate practical trial applications of the proposed simplified corner stress analysis procedures, a window-based computer program (ILLISTRS) was developed using Microsoft Visual Basic software package (Microsoft Taiwan Corp. 1995). The ILLISTRS program is a complete revision of the TKUPAV program (Lee 1999) for stress analysis with better control of graphical interfaces, selection menus, I/O file managements, and command buttons for efficiency and consistency. Both the English version and the Chinese version of the program are available at the following Web site: http://teg.ce.tku.edu.tw. Furthermore, since all the mechanistic variables used in the proposed models are dimensionally correct, the program can use both the imperial system and the metric system (SI). Example screens of the ILLISTRS program are shown in Fig. 6.

Discussions

The proposed stress analysis procedures follow a similar approach adopted by the NCHRP 1-26 report (Thompson et

Table 2. Additional prediction models for corner stress adjustments (after Lee and Lee 1996).

Dual wheel (single axle)	$R_1 = 0.6028 + 0.1338\Phi_1 + 0.00687\Phi_2$
	$\Phi_1 = \begin{cases} 0.548 + 0.861(A1) + 0.208(A1)^2 + 0.0176(A1)^3 & \text{if } A1 \le -2.0 \\ 2.963 + 4.594(A1) + 2.249(A1)^2 + 0.407(A1)^3 & \text{if } A1 > -2.0 \end{cases}$
	$\Phi_2 = \begin{cases} -0.382 - 0.364(A2) & \text{if } A2 \le -0.04 \\ 1.109 + 39.675(A2) & \text{if } A2 > -0.04 \end{cases}$
	$A1 = -0.986x1 + 0.00507x2 + 0.164x3 - 0.0121x4$
	$A2 = -0.0412x1 - 0.918x2 + 0.393x3 + 0.00129x4$
	$X = [x1, x2, x3, x4] = \left[\frac{s}{l}, \frac{a}{l}, \frac{sa}{l^2}, \frac{s}{a}\right]$
	Limits: $0.05 \le a/l \le 0.4$, $0 \le s/l \le 4$
Tandem axle (single wheel)	Same as the above equations; but
	$X = [x1, x2, x3, x4] = \left[\frac{t}{l}, \frac{a}{l}, \frac{ta}{l^2}, \frac{t}{a}\right]$
	Limits: $0.05 \le a/l \le 0.4$, $0 \le t/l \le 4$
Tridem axle (single wheel)	$R_1 = 0.4468 + 0.1679\Phi_1$
	$\Phi_1 = \begin{cases} -0.154 + 0.346(A1)^2 + 0.0986(A1)^2 + 0.0101(A3)^3 & \text{if } A1 \le -2.5 \\ 3.169 + 5.426(A1) + 2.880(A1)^2 + 0.528(A1)^3 & \text{if } A1 > -2.5 \end{cases}$
	$A1 = -0.9999x1 + 0.00576x2 - 0.0122x3$
	$X = [x1, x2, x3] = \left[\frac{t}{l}, \frac{a}{l}, \frac{t}{a}\right]$
	Limits: $0.05 \le a/l \le 0.4$, $0 \le t/l \le 4$
Tied concrete shoulder	$R_3 = 0.7543 + 0.1887\Phi_1 + 0.01840\Phi_2$
	$\Phi_1 = \begin{cases} 12.940 + 15.138(A1) + 5.305(A1)^2 + 0.604(A1)^3 & \text{if } A1 \le -2.55 \\ 1.321 + 0.154(A1) + 0.760(A1)^2 + 0.965(A1)^3 + 0.212(A1)^4 & \text{if } A1 > -2.55 \end{cases}$
	$\Phi_2 = 0.324 + 7.064(A2) + 7.003(A2)^2$
	$A1 = -0.531x1 + 0.636x2 - 0.560x3 + 0.00192x4$
	$A2 = -0.176x1 - 0.682x2 + 0.710x3 + 0.00639x4$
	$X = [x1, x2, x3, x4] = \left[\text{LAGG}, \frac{a}{l}, \frac{(\text{LAGG})a}{l}, \frac{(\text{LAGG})l}{a}\right]$
	where $\text{LAGG} = \log_{10}\left(1 + \frac{\text{AGG}}{kl}\right)$
Widened outer lane	$R_4 = 0.4429 + 0.1853\Phi_1 + 0.0335\Phi_2$
	$\Phi_1 = \begin{cases} 0.786 + 1.434(A1) + 0.463(A1)^2 + 0.0531(A1)^3 & \text{if } A1 \le -1 \\ 3.144 + 8.390(A1) + 7.674(A1)^2 + 2.667(A1)^3 & \text{if } A1 > -1 \end{cases}$
	$\Phi_2 = \begin{cases} -0.581 + 4.406(A2) + 16.204(A2)^2 & \text{if } A2 \le 0.1 \\ -0.408 + 4.209(A2) & \text{if } A2 > 0.1 \end{cases}$
	$A1 = -0.780x1 - 0.0597x2 + 0.662x3 - 0.00333x4$
	$A2 = 0.0524x1 - 0.781x2 + 0.622x3 - 0.00737x4$
	$X = [x1, x2, x3, x4] = \left(\frac{D_0}{l}, \frac{a}{l}, \frac{D_0 a}{l^2}, \frac{D_0}{a}\right)$
	Limits: $0.05 \le a/l \le 0.4$, $0 \le D_0/l \le 4$

al. 1992). The ILLI-CONC program can be used to calculate the slab edge stress for different axle load configurations. Nevertheless, "to estimate the combined stress due to load and temperature curling, some problems were encountered in analyzing the data using dimensional analysis". This paper enhanced the approach by resolving the dimensional analysis issue and providing a more complete treatment of the stress analysis at the slab corner. Stress adjustment factors (R), ranging from 0 to slightly greater than or equal to 1.0, are necessary when more practical pavement conditions such as finite slab sizes, different wheel load configurations, a widened outer lane, a second bonded or unbonded layer,

Fig. 6. Sample screens of the ILLISTRS program for stress analysis.

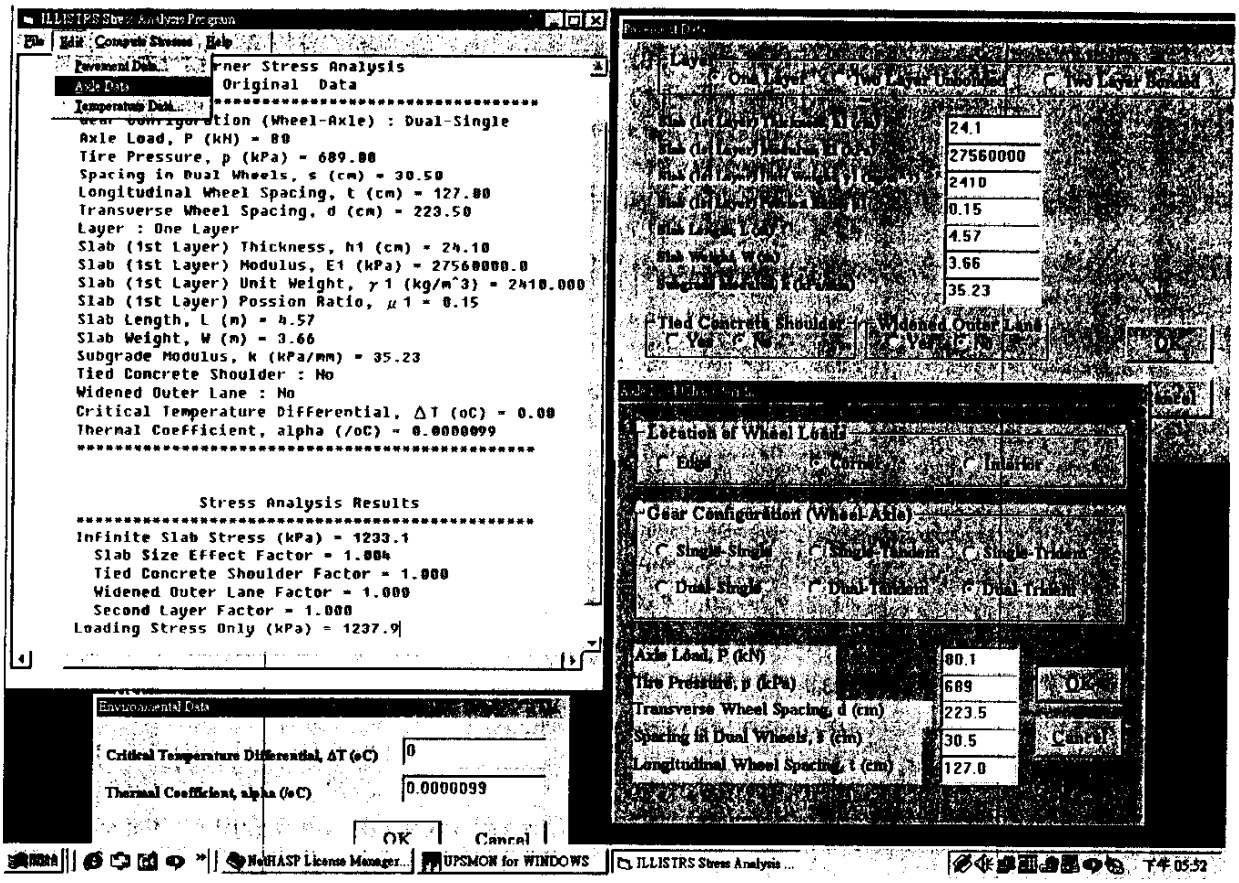

and thermal curling are considered. In reality, however, the presence of built-in curling at the time of construction may also have a significant effect on subsequent cracking. Readers should refer to other literature for a better understanding of such effects.

Conclusions

An alternative procedure for the determination of the critical corner stresses of jointed concrete pavements was developed in this study. The effects of a finite slab size, different wheel configurations, a widened outer lane, a tied concrete shoulder, a second bonded or unbonded layer, and thermal curling due to a linear temperature differential were considered. Specifically, the corner stress of a concrete slab due to the individual and combination effects of loading and nighttime curling was analyzed. A well-known slab-on-grade finite element program (ILLI-SLAB) was used for the analysis. A linear temperature differential across the slab thickness and a dense liquid foundation were assumed. The following conclusions and recommendations were drawn from this study:

1. The resulting minor principal (tensile) stresses of the ILLI-SLAB model occurring at the top of the slab corner favorably agree with Westergaard's closed-form solutions.
2. Additional tensile stresses may be induced at the top of the slab corner due to nighttime curling condition. Thus, the most critical corner stress condition due to the combination effects of loading and nighttime curling was considered.
3. The structural response characteristics of a slab corner were first investigated. The expected location of the maximum combined stresses due to corner loading plus curling was found within the Westergaard's location and the center of the slab along the corner angle bisector.
4. The corner stress along the line of a 1/4 circle centered at the very corner of the slab also shows about the same magnitude at most locations, which may help to explain the mechanism of the occurrence of corner breaks.
5. Based on the dimensionless mechanistic variables identified, a series of finite element factorial runs over a wide range of pavement designs was carefully selected and conducted. The resulting ILLI-SLAB corner stresses were compared with theoretical Westergaard solutions, and adjustment factors (R) were introduced to account for this discrepancy. Prediction equations for stress adjustments were developed using a modern regression technique (projection pursuit regression).
6. The critical location of minor principal stress may change from case to case due to the combination effect of loading plus thermal curling. The possibility of incorporating the location of critical stress occurrence into

the process of stress estimation should be further investigated.

7. A simplified corner stress analysis procedure was proposed and implemented in a user-friendly computer program (ILLISTRS) to facilitate instant stress estimations and practical trial applications.
8. Since all the mechanistic variables are dimensionless, the proposed prediction models can be utilized for both the U.S. customary system and the metric system.

Acknowledgments

This research work was sponsored by the National Science Council, Taiwan.

References

ASTM. 1993. Road and paving materials; pavement management technologies. Annual book of ASTM standards. Vol. 04.03, American Society for Testing and Materials, Philadelphia, Pa.

Bradbury, R.D. 1938. Reinforced concrete pavements. Wire Reinforcement Institute, Washington, D.C.

Darter, M.I., and Barenberg, E.J. 1977. Design of zero-maintenance plain jointed concrete pavement. Final Report, FHWA-RD-77-111, Vol. 1, Federal Highway Administration, Washington, D.C.

Darter, M.I., Hall, K.T., and Kuo, C.M. 1995. Support under portland cement concrete pavements. National Cooperative Highway Research Program Report 372, Transportation Research Board, National Research Council, Washington, D.C.

Friedman, J.H., and Stuetzle, W. 1981. Projection pursuit regression. Journal of the American Statistical Association, **76**: 817–823.

Hall, K.T., Darter, M.I., and Kuo, C.M. 1995. Improved methods for selection of k value for concrete pavement design. *In* Pavement monitoring and evaluation issues. Transportation Research Record 1505, Transportation Research Board, National Research Council, Washington, D.C., pp. 128–136.

Huang, Y.H. 1993. Pavement analysis and design. Prentice-Hall, Inc., Englewood Cliffs, N.J.

Ioannides, A.M. 1984. Analysis of slabs-on-grade for a variety of loading and support conditions. Ph.D. thesis, University of Illinois, Urbana, Ill.

Ioannides, A.M., Thompson, M.R., and Barenberg, E.J. 1985. The Westergaard solutions reconsidered. *In* Pavement system analysis. Transportation Research Record 1043, Transportation Research Board, National Research Council, Washington, D.C. pp. 13–23.

Korovesis, G.T. 1990. Analysis of slab-on-grade pavement systems subjected to wheel and temperature loadings. Ph.D. thesis, University of Illinois, Urbana, Ill.

Kuo, C.M. 1994. Three-dimensional finite element analysis of concrete pavement. Ph.D. thesis, University of Illinois, Urbana, Ill.

Lee, Y.H. 1999. TKUPAV: stress analysis and thickness design program for rigid pavements. ASCE Journal of Transportation Engineering, **125**(4): 338–346.

Lee, Y.H., and Darter, M.I. 1994*a*. Loading and curling stress models for concrete pavement design. *In* Design and rehabilitation of pavements. Transportation Research Record 1449, Transportation Research Board, National Research Council, Washington, D.C., pp. 101–113.

Lee, Y.H., and Darter, M.I. 1994*b*. New predictive modeling techniques for pavements. *In* Design and rehabilitation of pavements. Transportation Research Record 1449, Transportation Research Board, National Research Council, Washington, D.C., pp. 234–245.

Lee, Y.H., and Lee, Y.M. 1995. Theoretical investigation of corner stress in concrete pavements using dimensional analysis. Final Report, NSC83-0410-E032-009 and NSC84-2211-E032-022, National Science Council, Taipei, Taiwan. (In Chinese.)

Lee, Y.H., and Lee, Y.M. 1996. Corner stress analysis of jointed concrete pavements. *In* Rigid pavement design and rehabilitation issues. Transportation Research Record 1525, Transportation Research Board, National Research Council, Washington, D.C., pp. 44–56.

Lee, Y.H., Lee, Y.M., Yen, S.T., Bair, J.H., and Lee, C.T. 1996. Development of new stress analysis and thickness design procedures for jointed concrete pavements. Final Report (Phase II), NSC85-2211-E032-010, National Science Council, Taipei, Taiwan. (In Chinese.)

Lee, Y.H., Bair, J.H., Lee, C.T., Yen, S.T., and Lee, Y.M. 1997. Modified PCA stress analysis and thickness design procedures. *In* Pavement rehabilitation and design. Transportation Research Record 1568, Transportation Research Board, National Research Council, Washington, D.C., pp. 77–88.

Microsoft Taiwan Corp. 1994. Microsoft FORTRAN PowerStation Professional Development System: user's and reference manuals. Taipei, Taiwan.

Microsoft Taiwan Corp. 1995. Microsoft Visual Basic (version 4.0) programmer's guide and language reference. Taipei, Taiwan.

Salsilli-Murua, R.A. 1991. Calibrated mechanistic design procedure for jointed plain concrete pavements. Ph.D. thesis, University of Illinois, Urban, Ill.

Statistical Sciences, Inc. 1995. S-PLUS for Windows (version 3.3) user's manual and reference manual. Seattle, Wash.

Tabatabai-Raissi, A.M. 1977. Structural analysis of concrete pavement joints. Ph.D. thesis, University of Illinois, Urban, Ill.

Thompson, M.R., Barenberg, E.J., Carpenter, S.H., Darter, M.I., Dempsey, B.J., and Ioannides, A.M. 1990. Calibrated mechanistic structural analysis procedures for pavement. Final Report and Appendices, National Cooperative Highway Research Program 1-26, University of Illinois, Urbana, Ill.

Westergaard, H.M. 1926. Computation of stresses in concrete roads. Proceedings of the 5th Annual Meeting of the Highway Research Board, National Research Council, Washington, D.C., Part I, pp. 90–112.

Westergaard, H.M. 1927. Analysis of stresses in concrete pavements due to variations of temperature. Proceedings of the 6th Annual Meeting of the Highway Research Board, National Research Council, Washington, D.C., pp. 201–217.

List of symbols

a	radius of applied load, [L]
AGG	aggregate interlock factor, [FL^{-2}]
$a_m^{\Gamma}x$	lengths of projections
$a_1, a_2, \cdots, a_m$	direction vectors
B	finite slab width or length, [L]
C_1, C_2	curling stress coefficients for the desired and perpendicular directions
D_γ	relative deflection stiffness due to self-weight of concrete slab and possible loss of subgrade support
D_p	relative deflection stiffness due to external wheel load and loss of subgrade support
D_0	offset distance between the outer face of the wheel and the slab edge, [L]
E	modulus of elasticity of the concrete slab, [FL^{-2}]

E_1, E_2 concrete modulus of the top and the bottom slab, [FL^{-2}]
f_1 function of *a/l*, *L/l*, and *W/l*
f_2, f_3 functions for curling alone and curling plus loading, respectively
h thickness of the slab, [L]
h_{eff} effective thickness of a two-layer system, [L]
h_1, h_2 thickness of the top and the bottom slab, [L]
h_{1f}, h_{2f} equivalent top-layer thickness and bottom-layer thickness, [L]
I_{eff} equivalent moment of inertia of a unit-width section with modulus E_1, [L^3]
k modulus of subgrade reaction, [FL^{-3}]
l radius of relative stiffness, [L]
L, W finite slab length, [L]
M_T total bending moment of a two-layer system per unit width, [F]
p tire pressure, [FL^{-2}]
P total applied wheel load, [F]
R stress adjustment factor
R_T adjustment factor for the combined effect of loading plus nighttime curling (Case III) (note that adjustment factors R_T and R_{2b} should be used together for higher accuracy)
R_1 adjustment factor for different gear configurations
R_2 R_{2a} or R_{2b}
R_{2a} adjustment factor for finite slab length and width for loading-only condition (Case I)
R_{2b} adjustment factor for finite slab length and width for the condition of loading plus curling but $\Delta T = 0$ to allow partial contact at slab–subgrade interface (Case II)
R_3 adjustment factor for a tied concrete shoulder
R_4 adjustment factor for a widened outer lane
R_5 adjustment factor for a bonded/unbonded second layer
s transverse wheel spacing, [L]
t longitudinal axle spacing, [L]
W finite slab width, [L]
x location of the neutral axis at a distance fro the bottom of the second layer, [L]
x vector of predictor variables, $x = (x_1, x_2, \cdots x_p)^T$
X_1 distance to the point of maximum stress alon the corner angle bisector
$\bar{y}$ expected (or mean) value of response variabl
α thermal expansion coefficient, [T^{-1}]
α, β distances of the neutral axis from the middl surfaces of the second layer and the top laye respectively, [L]
β_m regression coefficient
γ unit weight of the concrete slab, [FL^{-3}]
ΔT linear temperature differential through the sla thickness, [T]
δ slab deflection, [L]
δ_{wc} critical corner deflection, [L]
ε residual or random error
μ Poisson's ratio of the concrete
σ, q slab bending stress and vertical subgrad stress, respectively, [FL^{-2}]
σ_c corner stress prediction, [FL^{-2}]
σ_{ce}, σ_{ci} edge and interior curling stresses, respectively [FL^{-2}]
σ_{ct} Bradbury's maximum curling stress, [FL^{-2}]
σ_{c0} Westergaard's interior curling stress for an infi nite slab, [FL^{-2}]
σ_{unbond}, σ_{bond} slab bending stress of two-layer unbonded an bonded systems, [FL^{-2}]
σ_{wc} Westergaard's closed-form corner stress solu tion, [FL^{-2}]
σ' slab bending stress of equivalent single layer [FL^{-2}]
σ_1, σ_2 top-layer and bottom-layer stresses, respec tively, [FL^{-2}]
$\phi_m(a_m^T x)$ nonparametric transformation functions of th projected lengths $a_m^T x$

Note that [F], [L], and [T] represent the primary dimensions fo force, length, and temperature, respectively.